https://doi.org/10.26682/sjuod.2020.23.2.49
Journal of University of Duhok, Vol.23, No.2 (Pure and Eng. Sciences), Pp 630-647, 2020 (Special Issue)

INVESTIGATION OF FLEXURAL PERFORMANCE OF CONCRETE BEAMS REINFORCED WITH GLASS FIBER REINFORCED POLYMER REBARS

MUHAMMAD **A**. **M**UHAMMAD [1,*], **F**ARIS **R**. **A**HMED[**] and **S**ERWAN **K**H. **R**AFIQ[*]
[*]Dept. of Civil Engineering, College of Engineering, University of Sulaimani, Kurdistan Region-Iraq
[**]Dept. of Civil Engineering, Faculty of Engineering, University OF Koya, Kurdistan Region-Iraq

(Accepted for Publication: December 8, 2020)

ABSTRACT

As a solution of steel corrosion, glass fiber reinforced polymer (GFRP) rebars have been recommended to be used as internal reinforcement instead of steel reinforcement during last two decades. Lightweight, no-corrosion, thermal conductivity, electrically and magnetically resistance, and higher tensile strength are main advantageous properties of GFRP rebars over steel reinforcement. However, it has been noted that the recommended design codes in this field still require modifications. Some studies were conducted on concrete structures reinforced with this new reinforcing material worldwide. In this paper, test data of fifty-three concrete beams reinforced with GFRP rebars were collected from eight different works to investigate cracking moment, nominal moment, deflection and neutral axis depth. The selected beams were reinforced with steel stirrups and GFRP rebars in traverse and longitudinal directions, respectively. The beams were tested under four-points loading test to fail in flexure. A comprehensive approach to calculate both experimental and predicted results is given in terms of deflection and flexural capacity. The experimental results are compared with calculated design results according to ACI 440.1R-15. Statistical data analysis is performed for both theoretical and experimental results. In conclusion, the multiplier factors for theoretical cracking moment, nominal moment, ultimate deflection and neutral axis depth have been proposed to be 0.94, 1.25, 1.4 and 0.806, respectively.

KEYWORDS: Concrete Beam; Glass Fiber Reinforced Polymer Rebar; Deflection; Moment Capacity; Four Point Loading Test; ACI 440.1R-15

Notation

a=depth of equivalent rectangular stress block, mm.	$M_{cr,exp}$=experimental moment capacity at first crack, $kN.m$.
A_f=total area of FRP reinforcement, mm^2.	M_n=nominal moment capacity at failure, $kN.m$.
$A_{f,min}$=minimum area of FRP reinforcement, mm^2.	$M_{n,exp}$=experimental moment capacity at failure, $kN.m$.
b=width of beam, mm.	n_f=ratio of elastic modulus of FRP rebars to that of concrete.
c=distance between top fiber and neutral axis, mm.	P_{cr}= load at first crack, kN.
c_b=distance between top fiber and neutral axis at balanced strain, mm.	$P_{cr,exp}$ = experimental load at first crack, kN.
c_{exp}= experimental distance between top fiber and neutral axis, mm.	P_n= nominal load at failure, kN.
d=distance between top fiber and centroid of FRP reinforcement, mm.	$P_{n,exp}$=experimental load at failure, kN.
E_c=elastic modulus of concrete, MPa.	y_t=distance from centroidal gross section to bottom face, mm.
E_f=elastic modulus of FRP rebars, GPa.	β_1= rectangular concrete stress height to neutral axis depth ratio
f_c'= cylinder compressive strength of concrete, MPa.	Δ_{cr}=middle span deflection at first crack, mm.

: muhammad.rashid@univsul.edu.iq; faris.rashied@koyauniversity.org; serwan.rafiq@univsul.edu.iq
[1]Corresponding author: College of Engineering, University of Sulaimani, Kurdistan Region, Iraq.

f_{fu}= tensile strength of FRP rebars, MPa.	$\Delta_{cr,exp}$=experimental middle span deflection at first crack, mm.
$f_{f,exp}$= experimental tensile stress in FRP rebars, MPa.	Δ_n= middle span deflection at failure, mm.
f_r=flexural strength of concrete, MPa.	$\Delta_{n,exp}$= experimental middle span deflection at failure, mm.
h=height of beam, mm.	ε_c= strain in concrete.
I_{cr}=moment of inertia of transformed cracked beam, mm^4.	$\varepsilon_{c,exp}$= experimental strain in concrete.
I_e=effective moment of inertia of beam, mm^4.	ε_{cu}= ultimate strain in concrete.
$I_{e,exp}$=experimental effective moment of inertia of beam, mm^4.	$\varepsilon_{cu,exp}$= experimental ultimate strain in concrete.
I_g=gross moment of inertia of beam, mm^4.	ε_f= strain in FRP rebars.
k=ratio of neutral axis depth to FRP reinforcement depth.	$\varepsilon_{f,exp}$= experimental strain in FRP rebars.
L=total length of beam, mm.	ε_{fu}= ultimate strain in FRP rebars.
L_n=span length of beam supports, mm.	$\varepsilon_{fu,exp}$= experimental ultimate strain in FRP rebars.
L_s=shear span length from point loads to beam supports, mm.	γ= variation factor in stiffness.
L_b=pure bending span length between point loads, mm.	λ= lightweight concrete factor.
L_o=overhanging length between support and free end, mm.	α=concrete strength reduction factor
M_a=applied moment, $kN.m$.	ρ_f=FRP reinforcement ratio.
M_{cr}=moment capacity at first crack, $kN.m$.	ρ_{fb}=FRP reinforcement ratio at balanced strain.

1. INTRODUCTION

Over the world numerous steel reinforced concrete structures have been exposed to steel corrosion in serious environments and structural deterioration resulting in expensive rehabilitation and lockdown of facilities. To solve corrosion issue, the use of glass fiber reinforced polymer (GFRP) bars as internal reinforcement has developed as a promising alternative of traditional steel reinforcement. Besides noncorrosive nature of GFRP rebars, they also have high tensile strength, lightweight, lower thermal conductivity, electromagnetic neutrality, and these advantages over steel make GFRP attractive as internal reinforcement to be applied in concrete structures.

Reinforced concrete members with GFRP perform differently from those reinforced with steel. GFRP rebars have linear stress strain relationship up to GFRP rupture, and resulting in sudden structural failure without warning. In addition, modulus of elasticity of the GFRP bars is lower than that of steel (Bank 2006). Therefore, for the same reinforcement ratio, reinforced concrete members with GFRP comparing to steel have greater deflection and crack widths (Tighiouart et al 1998). Hence, the design of GFRP reinforced concrete members is typically governed by serviceability requirements more than strength requirements. Owing to the brittle behavior of GFRP rebar and concrete, it is recommended to predict moment capacity with concrete mode of failure than GFRP rupture to avoid sudden collapse because concrete crushing is more progressive and resulting in less catastrophic failure (ACI Committee 440 2015).

GFRP rebars has been commonly manufactured for concrete reinforcement over the last two decades. Annual estimated amount of FRP used in construction is over 10 million meters (Burgoyne et al 2007). Many GFRP plants are a commercially available to produce GFRP rebar, which are mostly on request demand. Due to the dispersion of FRP market and lack of well-founded international standards, a wide range of GFRP products are existing on the market (Emparanza et al 2018). The GFRP products have a wide range of surface texture, such as smooth, helically deformed, warped, ribbed, sand coated, which affects the bonding

: muhammad.rashid@univsul.edu.iq; faris.rashied@koyauniversity.org; serwan.rafiq@univsul.edu.iq
[1]Corresponding author: College of Engineering, University of Sulaimani, Kurdistan Region, Iraq.

behaviors. In addition, GFRP rebars have also different mechanical properties are such as tensile strength and modulus of elasticity. On the other hand, Most of GFRP design codes and guides use those equations applied for steel reinforced concrete members with some amendments to comprise the alterations in the mechanical properties between GFRP and steel rebars. Therefore, establishing equations to find the GFRP performance may produce reasonable estimates with one type of FRP bars but disagreements with another type.

Over the last decades, a number of research studies were carried out to the flexural performance of GFRP reinforced concrete beams (Benmokrane et al 1995; Alsayed et al 2000; Toutanji & Saafi, 2000; Ashour 2006; Kalpana & Subramanian 2011; Goldston et al 2016; El-Nemr et al 2018). In these studies, the effects of normal and high strength concrete on the flexural behavior of GFRP reinforced beams were investigated. In addition, GFRP configuration, reinforcement ratio, different GFRP rebar with different mechanical properties have been considered as experimental parameters. In the study case of deflections, some coefficients were proposed to predict the effective moment of inertia concrete beams reinforced with GFRP rebar (Bischoff 2005). It was reported that ACI 440 calculations predicted conservative ultimate moment and underestimated failure deflections as well. however, these predictions vary among research studies. This paper covers the deflection and flexural moment capacity of concrete beams reinforced with GFRP rebar as longitudinal flexural reinforcement and steel stirrups. The database was made to collect the pure bending test data of 53 GFRP reinforced beams from 8 different experimental studies. The beams were theoretically designed according to the design recommendations in ACI 440.1R-15. Experimental test results were also compared with those of the theoretical design to investigate the applicability of the code.

2.Experimental Database

The results of 53 concrete beam reinforced with GFRP rebars were collected from eight different research studies from the literature (Toutanji and Deng 2003; Barris et al 2009; Wang and Belarbi 2011; Kassem et al 2011; Adam et al 2015; Goldston et al 2016; El-Nemr et al 2018; El Refai et al 2015). The beams were tested under four points flexural test at the age of 28 days. The beams cover a variety of dimensions whereas the instrumental schematic side view of tested beams was similar as shown in Figure 1. All beams were designed with adequate shear resistance using steel stirrups and expected to fail in flexure. Table 1 presents the GFRP rebars and concrete properties used in the beams design. GFRP rebars had different diameters ranged between (6.35-25) mm. The reinforcement area was computed according to the actual bar diameter instead of using nominal area. GFRP modulus of elasticity and tensile strength also vary between (30-69) GPa, (551-1764) MPa, respectively. Furthermore, the compressive strengths of concrete included in the database differs from 20 MPa to 80 MPa. Table 2 gives the GFRP flexural reinforcement detail and dimensional properties for each beam. The beams had various total length and clear span ranges between (2032-4250) mm and (1800-3750) mm, respectively. The beams have two kind of reinforcement arrangements in one or two layers, and their effective depth calculated from extreme compression fiber to the centroid of GFRP rebar according to moment of areas of bars. The rate of loading had been strain controlled (deflection rate per time) or load controlled (load increments). Rates of loading for strain controlled differed from 0.6 to 1.2 mm/min while for load controlled ranged between 13 to 70 increments.

: muhammad.rashid@univsul.edu.iq; faris.rashied@koyauniversity.org; serwan.rafiq@univsul.edu.iq

[1]Corresponding author: College of Engineering, University of Sulaimani, Kurdistan Region, Iraq.

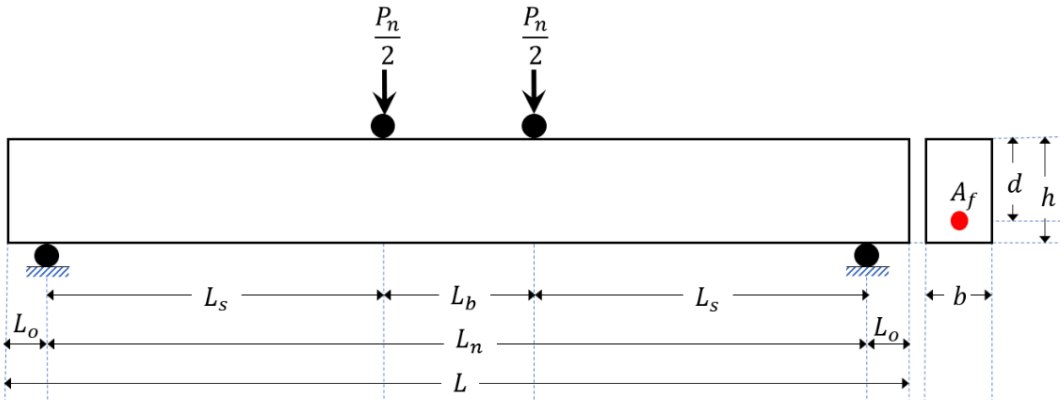

Fig. (1): Beam instrumental setup for four points loading test

Table (1): GFRP rebar and concrete mechanical properties used in test beams

Reference	Beam ID	GFRP rebar properties						Concrete properties	
		Dia. mm	A_f, mm^2	E_f, GPa	f_{fu}, MPa	ε_{fu}, mm/mm	Surface texture	f_c, MPa	E_c, MPa
Kassem et al (2011)	G1-6	12.7	760	40.0	617	0.0150	sand coat	39.05	29300
	G1-8	12.7	1013	40.0	617	0.0150	sand coat	39.05	29300
	G2-6	12	679	36.0	747	0.0180	Ribbed deformed	39.05	29300
	G2-8	12	905	36.0	747	0.0180	Ribbed deformed	39.05	29300
El-Nemr et al (2018)	3#13G1	13	398	48.7	817	0.0170	sand coated	33.5	27203
	5#13G1	13	664	48.7	817	0.0170	sand coated	38.95	29333
	2#13G2	13	265	67.0	1639	0.0250	sand coated	33.5	27203
	3#15G1	15.9	596	48.1	751	0.0160	sand coated	38.95	29333
	4#15G1	15.9	794	48.1	751	0.0160	sand coated	38.95	29333
	2#15G2	15.9	397	69.3	1362	0.0200	sand coated	29	25310
	2#15G3	15.9	397	59.5	1245	0.0210	helically grooved	33.83	27337
	6#15G1	15.9	1191	48.1	751	0.0160	sand coated	33.5	27203
	5#15G2	15.9	993	69.3	1362	0.0200	sand coated	29	25310
	5#15G3	15.9	993	59.5	1245	0.0210	helically grooved	33.8	27325
	2#20G1	20	628	47.6	728	0.0150	sand coated	38.95	29333
	3#20G1	20	942	47.6	728	0.0150	sand coated	42.1	30496
	2#22G1	22	760	46.4	693	0.0150	sand coated	38.95	29333
	3#20G2	20	942	52.5	1082	0.0210	sand coated	48.13	32607
	2#25G1	25	982	53.2	666	0.0130	sand coated	48.13	32607
	2#25G2	25	982	66.3	1132	0.0170	sand coated	48.13	32607
	2#25G3	25	982	60.3	906	0.0150	helically grooved	33.8	27325
Wang and Belarbi (2011)	P4G-1	13	664	41.0	690	0.0168	sand coated	48	32563
	P8G-1	25	982	41.0	551	0.0134	sand coated	48	32563
Toutanji and	GB1-1	12.7	253	40.0	695	0.0174	NG	35	35000

: muhammad.rashid@univsul.edu.iq; faris.rashied@koyauniversity.org; serwan.rafiq@univsul.edu.iq
[1]Corresponding author: College of Engineering, University of Sulaimani, Kurdistan Region, Iraq.

Deng (2003)	GB1-2	12.7	253	40.0	695	0.0174	NG	35	35000
	GB2-1	12.7	380	40.0	695	0.0174	NG	35	35000
	GB2-2	12.7	380	40.0	695	0.0174	NG	35	35000
	GB3-1	12.7	507	40.0	695	0.0174	NG	35	35000
	GB3-2	12.7	507	40.0	695	0.0174	NG	35	35000
El Refai et al (2015)	2G12	12	226	50.0	1000	0.0200	NG	40	29725
	3G12	12	339	50.0	1000	0.0200	NG	40	29725
	3G16	16	603	50.0	1000	0.0200	NG	40	29725
Barris et al (2009)	C-212-D1	12	226	63.3	1353	0.0210	spirally ribbed	59.8	26939
	C-216-D1	16	402	64.2	995	0.0160	spirally ribbed	56.3	26524
	C-316-D1	16	603	64.2	995	0.0160	spirally ribbed	55.3	24926
	C-212-D2	12	226	63.3	1353	0.0210	spirally ribbed	39.6	23163
	C-216-D2	16	402	64.2	995	0.0160	spirally ribbed	61.7	27318
	C-316-D2	16	603	64.2	995	0.0160	spirally ribbed	60.1	26910
Goldston et al (2016)	40-#2-0.5-S	6.35	63	37.5	732	0.0196	NG	40	29725
	40-#3-1.0-S	9.53	143	55.6	1764	0.0318	NG	40	29725
	40-#4-2.0-S	12.7	253	48.6	1605	0.0330	NG	40	29725
	80-#2-0.5-S	6.35	63	37.5	732	0.0196	NG	80	42038
	80-#3-1.0-S	9.53	143	55.6	1764	0.0318	NG	80	42038
	80-#4-2.0-S	12.7	253	48.6	1605	0.0330	NG	80	42038
Adam et al (2015)	A25-1	8	101	30.0	640	0.0200	Ribbed deformed	19.6	20808
	A25-2	8,12	163	30.0	640	0.0200	Ribbed deformed	19.6	20808
	A25-3	8,12	277	30.0	640	0.0200	Ribbed deformed	19.6	20808
	A45-1	8,12	163	30.0	640	0.0200	Ribbed deformed	38.4	29125
	A45-2	8,12	277	30.0	640	0.0200	Ribbed deformed	38.4	29125
	A45-3	12	452	30.0	640	0.0200	Ribbed deformed	38.4	29125
	A70-1	8,12	277	30.0	640	0.0200	Ribbed deformed	59.52	36260
	A70-2	12	452	30.0	640	0.0200	Ribbed deformed	59.52	36260
	A70-3	12	679	30.0	640	0.0200	Ribbed deformed	59.52	36260

Table (2):GFRP rebar configuration, GFRP reinforcement ratios and test beam dimensions

Reference	Beam ID	GFRP rebar Configuration	L, mm	b, mm	h, mm	L_n, mm	L_s, mm	d, mm	ρ_f, %	ρ_{fb}, %
Kassem et al (2011)	G1-6	6#12.7mm – 2 rows	3300	200	300	2750	875	232	1.64	0.68
	G1-8	8#12.7mm – 2 rows	3300	200	300	2750	875	232	2.18	0.68
	G2-6	6#12mm – 2 rows	3300	200	300	2750	875	233	1.46	0.43
	G2-8	8#12mm – 2 rows	3300	200	300	2750	875	233	1.94	0.43
El-Nemr et al (2018)	3#13G1	3#13mm – 1 row	4250	200	400	3750	1375	354	0.56	0.43
	5#13G1	5 #13mm – 1 row	4250	200	400	3750	1375	344	0.97	0.47
	2#13G2	2 #13mm – 1 row	4250	200	400	3750	1375	344	0.39	0.15

: muhammad.rashid@univsul.edu.iq; faris.rashied@koyauniversity.org; serwan.rafiq@univsul.edu.iq

[1]Corresponding author: College of Engineering, University of Sulaimani, Kurdistan Region, Iraq.

	3#15G1	3#15.9mm – 1 row	4250	200	400	3750	1375	343	0.87	0.55
	4#15G1	4#15.9mm – 1 row	4250	200	400	3750	1375	343	1.16	0.55
	2#15G2	2#15.9mm – 1 row	4250	200	400	3750	1375	343	0.58	0.20
	2#15G3	2#15.9mm – 1 row	4250	200	400	3750	1375	343	0.58	0.23
	6#15G1	6#15.9mm – 2 rows	4250	200	400	3750	1375	320	1.86	0.50
	5#15G2	5#15.9mm – 2 rows	4250	200	400	3750	1375	331	1.50	0.20
	5#15G3	5#15.9mm – 2 rows	4250	200	400	3750	1375	331	1.50	0.23
	2#20G1	2# 20mm – 1 row	4250	200	400	3750	1375	340	0.92	0.58
	3#20G1	3#20mm – 1 row	4250	200	400	3750	1375	340	1.39	0.60
	2#22G1	2#22mm – 1 row	4250	200	400	3750	1375	339	1.12	0.62
	3#20G2	3#20mm – 1 row	4250	200	400	3750	1375	340	1.39	0.34
	2#25G1	2#25mm–1 row	4250	200	400	3750	1375	338	1.45	0.84
	2#25G2	2#25mm – 1 row	4250	200	400	3750	1375	338	1.45	0.38
	2#25G3	2#25mm – 1 row	4250	200	400	3750	1375	338	1.45	0.43
Wang and	P4G-1	5 #13mm – 1 row	2032	178	229	1828	711	185	2.02	0.63
Belarbi (2011)	P8G-1	2 #25mm – 1 row	2032	178	229	1828	711	178	3.09	0.96
Toutanji and	GB1-1	2#12.7mm – 1 row	3000	180	300	2800	1200	268	0.53	0.50
Deng (2003)	GB1-2	2#12.7mm – 1 row	3000	180	300	2800	1200	268	0.53	0.50
	GB2-1	3#12.7mm – 1 row	3000	180	300	2800	1200	268	0.79	0.50
	GB2-2	3#12.7mm – 1 row	3000	180	300	2800	1200	268	0.79	0.50
	GB3-1	4#12.7mm – 2 row	3000	180	300	2800	1200	255	1.10	0.50
	GB3-2	4#12.7mm – 2 row	3000	180	300	2800	1200	255	1.10	0.50
El Refai et al	2G12	2#12mm – 1 row	4000	230	300	3700	1250	244	0.40	0.34
(2015)	3G12	3#12mm – 1 row	4000	230	300	3700	1250	244	0.60	0.34
	3G16	3#16mm – 1 row	4000	230	300	3700	1250	242	1.08	0.34
Barris et al	C-212-D1	2#12mm – 1 row	2050	140	190	1800	600	163	0.99	0.30
(2009)	C-216-D1	2#16mm – 1 row	2050	140	190	1800	600	162	1.77	0.51
	C-316-D1	3#16mm – 1 row	2050	140	190	1800	600	162	2.66	0.50
	C-212-D2	2#12mm – 1 row	2050	160	190	1800	600	143	0.99	0.23
	C-216-D2	2#16mm – 1 row	2050	160	190	1800	600	141	1.78	0.56
	C-316-D2	3#16mm – 1 row	2050	160	190	1800	600	141	2.67	0.54
Goldston et al	40-#2-0.5-S	2#6.35mm – 1 row	2400	100	150	2000	667	128	0.50	0.47
(2016)	40-#3-1.0-S	2#9.53mm – 1 row	2400	100	150	2000	667	126	1.13	0.13
	40-#4-2.0-S	2#12.7mm – 1 row	2400	100	150	2000	667	125	2.03	0.13
	80-#2-0.5-S	2#6.35mm – 1 row	2400	100	150	2000	667	128	0.50	0.80
	80-#3-1.0-S	2#9.53mm – 1 row	2400	100	150	2000	667	126	1.13	0.22
	80-#4-2.0-S	2#12.7mm – 1 row	2400	100	150	2000	667	125	2.03	0.23
Adam et al	A25-1	2#8mm – 1 row	2800	120	300	2500	1100	250	0.34	0.27
(2015)	A25-2	1#12mm + 1#8mm	2800	120	300	2500	1100	250	0.54	0.27
	A25-3	2#12mm + 1#8mm	2800	120	300	2500	1100	250	0.92	0.27

: muhammad.rashid@univsul.edu.iq; faris.rashied@koyauniversity.org;
serwan.rafiq@univsul.edu.iq
[1]Corresponding author: College of Engineering, University of Sulaimani, Kurdistan Region, Iraq.

A45-1	1#12mm + 1#8mm	2800	120	300	2500	1100	250	0.54	0.49
A45-2	2#12mm + 1#8mm	2800	120	300	2500	1100	250	0.92	0.49
A45-3	4#12mm – 2 row	2800	120	300	2500	1100	250	1.51	0.49
A70-1	2#12mm + 1#8mm	2800	120	300	2500	1100	250	0.92	0.63
A70-2	4#12mm – 2 row	2800	120	300	2500	1100	250	1.51	0.63
A70-3	6#12mm – 2 row	2800	120	300	2500	1100	244	2.32	0.63

3. METHODOLOGY

3.1. Flexural Moment Capacity

The theoretical method explained below is based on the recommendations reported by ACI Committee 440 (2015). All 53 beams tested were simply supported and designed to follow one of the three failure modes. Tension control in bottom of the beam where GFRP rebars ruptured during loading or compression control in top of the beam where concrete failure occurs up to reaching ultimate compressive strain. The beam may fail in both tension and compression simultaneously, which is called balanced failure. Classification of failure modes depends on the provided reinforcement ratio ρ_f and the balanced reinforcement ratio ρ_{fb} as given in Equation (1) and (2), respectively. When $\rho_f < \rho_{fb}$, the beam will fail in tension. When $\rho_f > \rho_{fb}$, top fiber of concrete was expected to suffer crushing failure. in case of $\rho_f = \rho_{fb}$, the failure mode is expected to be balanced failure. It was reported that failure in GFRP or concrete is catastrophic without warning. According to ACI Committee 440 (2015), it is recommended to design beams with concrete crushing more than GFRP failure. The theoretical concrete compressive strain $\varepsilon_{cu} = 0.003$ is taken into account as the ultimate compressive strain.

$$\rho_f = \frac{A_f}{bd}$$

$$\rho_{fb} = 0.85\beta_1 \frac{f_c'}{f_{fu}} \frac{E_f \varepsilon_{cu}}{E_f \varepsilon_{cu} + f_{fu}}$$

The actual flexural compressive concrete stress distribution above the neural axis is nonlinear and in practice it is awkward to use this distribution. Therefore, the actual stress distribution is substituted by an equivalent rectangular concrete stress block by using cylindrical concrete compressive strength reduction factor $\alpha = 0.85$ and the equivalent block depends on both concrete strength reduction factor α , and β_1 which is the ratio between equivalent rectangular concrete compressive stress height a to neutral axis depth c. The value of $\alpha = 0.85$ and Equation (3) to determine β_1 were adopted from ACI Committee 318 (2019).

: muhammad.rashid@univsul.edu.iq; faris.rashied@koyauniversity.org; serwan.rafiq@univsul.edu.iq
[1]Corresponding author: College of Engineering, University of Sulaimani, Kurdistan Region, Iraq.

$$\beta_1 = \begin{cases} 0.85 & \text{for } 17 \text{ MPa} \le f_c' \le 28 \text{ MPa} \\ 0.85 - 0.05\left(\frac{f_c' - 28}{7}\right) & \text{for } 28 \text{ MPa} < f_c' \le 55 \text{ MPa} \\ 0.65 & \text{for } f_c' > 55 \text{ MPa} \end{cases}$$

For compression control ($\rho_f > \rho_{fb}$), theoretical nominal moment capacity is calculated by Equation (4) and the depth of rectangular concrete stress block is calculated using Equation (5). The actual tensile stress in GFRP rebars can be calculated as given in Equation (6), which is less than of its ultimate tensile strength. neutral axis depth c from extreme compression fiber is found using Equation (7). The actual GFRP tensile strain is also calculated from Equation (8), which is corresponding to the theoretical ultimate concrete strain. The governing equations follow the same assumptions of the flexural theory used for conventional reinforced concrete beams. It can be noted that while $\rho_f > \rho_{fb}$, minimum area of GFRP rebars $A_{f,min}$ is not required to be checked because the compression controlled failure governs the situation where the actual provided reinforcement area is greater than that of minimum limit from Equation (13).

$$M_n = A_f f_f \left(d - \frac{a}{2}\right) \quad (4)$$

$$a = \frac{A_f f_f}{0.85 f_c' b}$$

$$f_f = \left(\sqrt{\frac{\left(E_f \varepsilon_{cu}\right)^2}{4} + \frac{0.85\beta_1 f_c'}{\rho_f} E_f \varepsilon_{cu}} - 0.5 E_f \varepsilon_{cu}\right) \le f_{fu} \quad (6)$$

$$c = \frac{a}{\beta_1}$$

$$\varepsilon_f = \left(\frac{d - c}{c}\right) \varepsilon_{cu}$$

For tension control *($\rho_f < \rho_{fb}$),* nominal moment capacity M_n is calculated by Equation (9), where ultimate FRP tensile strength used as GFRP rupture occurs. Concrete stress block depth a can be found from Equation (10). However, *Equation (9)&(10) are not recommended because of unknowns of the actual concrete strain* concrete ε_c , and *equivalent stress block parameters* α and β_1. As a result, nominal moment strength for tension control beams are conservatively computed similar to that of balanced failure conditions, where

: muhammad.rashid@univsul.edu.iq; faris.rashied@koyauniversity.org; serwan.rafiq@univsul.edu.iq
[1]Corresponding author: College of Engineering, University of Sulaimani, Kurdistan Region, Iraq.

$\varepsilon_{cu} = 0.003$ and ε_{fu} used as given in Equation (11) & (12). Here, it is necessary to provide beams with FRP reinforcements not less than minimum GFRP reinforcement ratio, which can be found using Equation (13).

$$M_n = A_f f_{fu}\left(d - \frac{a}{2}\right) \quad (9)$$

$$a = \frac{A_f f_{fu}}{0.85 f_c' b} \quad (10)$$

$$M_n = A_f f_{fu}\left(d - \frac{\beta_1 c_b}{2}\right) \quad (11)$$

$$c_b = \left(\frac{\varepsilon_{cu}}{\varepsilon_{cu} + \varepsilon_{fu}}\right) d \quad (12)$$

$$A_{f,min} = \frac{0.41\sqrt{f_c'}}{f_{fu}} b_w d \geq \frac{2.3}{f_{fu}} bd \quad (13)$$

From experimental point of view, the applied loads at failure $P_{n,exp}$ were recorded during flexural beam test. and the dimensions were also measured. The experimental flexural moment capacity at midspan $M_{n,exp}$ was calculated using Equation (14) based on Euler–Bernoulli beam theory.

$$M_{n,exp} = \frac{P_{n,exp}}{2} L_s \quad (14)$$

3.2. Cracking moment

Cracking moment symbolized as M_{cr} is defined as the moment, which causes the first crack of concrete beam. The calculation of the cracking moment depends on flexural strength of concrete f_r, gross moment of inertia I_g and distance between centroid of the section and extreme tension fiber, $y_t = h/2$. The flexural strength of concrete was computed in terms of concrete compressive strength according Equation (15), where lightweight concrete factor $\lambda = 1$ for normal concrete. For rectangular section, the value of $y_t = h/2$ and I_g is calculated as given in Equation (16). As a result, Equation (17) was is used to find the predicted cracking moment.

: muhammad.rashid@univsul.edu.iq; faris.rashied@koyauniversity.org; serwan.rafiq@univsul.edu.iq

[1]Corresponding author: College of Engineering, University of Sulaimani, Kurdistan Region, Iraq.

f_r

$$= 0.62\lambda\sqrt{f_c'} \quad (15)$$

I_g

$$= \frac{bh^3}{12} \quad (16)$$

M_{cr}

$$= \frac{f_r I_g}{y_t} \quad (17)$$

It is noted that experimental cracking loads were reported in the literature. For the calculation of the experimental cracking moment $M_{cr,exp}$, while the first crack appeared on concrete beam the applied loads at first crack $P_{cr,exp}$ were documented. The experimental cracked moment at midspan was computed using Equation (18).

$M_{cr,exp}$

$$= \frac{P_{cr,exp}}{2} L_s \quad (18)$$

3.3. Ultimate Deflection

The Euler–Bernoulli formula describes the relationship between the beam stiffness EI and the internal moment M as given in Equation (19). It is simplified by taking double integration to calculate elastic deflection along the beam length while moment and stiffness are constant.

$$\frac{d^2\Delta}{dx^2} = \frac{M}{EI} \quad (19)$$

Due to concrete cracking while loading, the beam stiffness will vary because of decrease in moment of inertia I up to beam failure. Therefore, the elastic deflection depends on the varying moment of inertia called effective moment of inertia I_e and its corresponding moment M_a. I_e varies between gross moment of inertia of uncracked section I_g and cracked moment of inertia section I_{cr}. has a moment of inertia equal to the gross moment of inertia, Ig. The stiffness also differs along the length of beam and the variation stiffness factor γ was reported by Bischoff (2005) adopted by ACI 440 to include this variation. Equations (20) to (25) governs the calculation of I_e according to elastic analysis of transferred beam composite section.

$$I_{cr} = \frac{bd^3}{3} k^3 + n_f A_f d^2 (1 - k)^2 \quad (20)$$

: muhammad.rashid@univsul.edu.iq; faris.rashied@koyauniversity.org; serwan.rafiq@univsul.edu.iq
[1]Corresponding author: College of Engineering, University of Sulaimani, Kurdistan Region, Iraq.

$$n_f = \frac{E_f}{E_c} \quad (21$$

$$E_c = 4700\sqrt{f_c'} \quad (2$$

$$k = \sqrt{2\rho_f n_f + (\rho_f n_f)^2} - \rho_f n_f \quad (23)$$

$$\gamma = 1.72 - 0.72\left(\frac{M_{cr}}{M_a}\right) \quad (24)$$

$$I_e = \frac{I_{cr}}{1 - \gamma\left(\frac{M_{cr}}{M_a}\right)^2\left[1 - \frac{I_{cr}}{I_g}\right]} \leq I_g \quad (25)$$

Theoretical midspan deflection Δ_n at max flexural capacity was calculated when $M_a = M_n$. For four point loading test, from Equation (25) the ultimate loads were computed from moment capacities. Finally, Δ_n can be obtained by applying Equation (27).

$$P_n = \frac{2M_n}{L_s} \quad (26)$$

$$\Delta_n = \frac{P_n L_s}{48E_c I_e}(3{L_n}^2 - 4{L_s}^2) \quad (27)$$

During flexural beam tests, the experimental deflections at midspan $\Delta_{n,exp}$ were observed using the LVDT sensors while the concrete failure or FRP rupture occurred at its conforming $M_{n,exp}$.

3.4. First Crack Deflection

First crack deflection occurs when the applied moment $M_a = M_{cr}$ and $I_e = I_g$. Beyond M_{cr}, concrete beam start cracking. The cracking load P_{cr} and theoretical elastic cracking deflection Δ_{cr} can be calculated from Equation (28) & (29), respectively.

$$P_{cr} = \frac{2M_{cr}}{L_s} \quad (28)$$

$$\Delta_{cr} = \frac{P_{cr} L_s}{48E_c I_g}(3{L_n}^2 - 4{L_s}^2) \quad (29)$$

Regarding the investigational values, while the first crack occurs at $P_{cr,exp}$, experimental cracking deflection $\Delta_{cr,exp}$ were recorded at midspan of the beam.

3.5. Neural Axis Depth

The theoretical neutral axis depth c was

: muhammad.rashid@univsul.edu.iq; faris.rashied@koyauniversity.org; serwan.rafiq@univsul.edu.iq
[1]Corresponding author: College of Engineering, University of Sulaimani, Kurdistan Region, Iraq.

found from Equation (7) for concrete crushing & (12) for GFRP rupture, which was assumed $\varepsilon_{cu} = 0.003$. The experimental depth of the neutral axis was calculated by Equation (30). Strain gauges were attached on the top of concrete beam and FRP rebars at midspan to measure $\varepsilon_{cu,exp}$ and $\varepsilon_{f,exp}$, respectively. The effective beam depth d calculated from top of the beam to centroid of GFRP reinforcements.

$$c_{exp} = \left(\frac{\varepsilon_{cu,exp}}{\varepsilon_{cu,exp} + \varepsilon_{f,exp}}\right) d \quad (30)$$

4. RESULTS AND DISCUSSION

Table 3 compares the results obtained from the literature and those calculated by ACI 440 recommendations for each beam. Due to a wide series of beam specimens and different materials properties, the data were fluctuated among those reported by the studies. However, the variations do not significantly affect the general trend. The common failure modes were concrete crushing as a consequence of $\rho_f > \rho_{fb}$. The beams of 2G12, , A25-1, A45-1, A70-1 were failed at GFRP rupture mode while their ρ_f/ρ_{fb} ratio were 1.19, 1.23, 1.11 and 1.46, respectively. It is expected by ACI 440 that FRP rupture may occur at reinforcement ratio up to $1.4\,\rho_{fb}$. Accordingly, it can be suggested to start designing GFRP reinforced concrete member with $\rho_f = 1.5\rho_{fb}$ to avoid tension failure.

Table (3): Experimental values against ACI 440.1R.15 design

		Experimental							ACI 440.1R.15			
Reference	Beam ID	$M_{cr,exp}$ $kN.m$	$M_{n,exp}$ $kN.m$	$\Delta_{n,exp}$ mm	$\varepsilon_{f,exp}$ με	$\varepsilon_{cu,exp}$ με	c_{exp} mm	failure mode	c mm	M_{cr} $kN.m$	M_n $kN.m$	Δ_n mm
Kassem et al (2011)	G1-6	10.92	77.47	51.8	12436	3269	48	C.C	56	11.62	60.44	37.6
	G1-8	11.37	86.76	48	11240	3210	52	C.C	63	11.62	67.41	33.2
	G2-6	11.15	71	50.8	14400	3100	41	C.C	51	11.62	55.73	41.3
	G2-8	11.34	84.54	50.3	11470	3150	50	C.C	58	11.62	62.37	36.5
El-Nemr et al (2018)	3#13G1	13.46	81.34	64.2	13726	1561	36	C.C	61	19.14	92.23	62.0
	5#13G1	15.26	130.6	76.8	15095	1933	39	C.C	72	20.64	115.87	52.9
	2#13G2	13.75	82.78	71.7	16359	2541	46	C.C	57	19.14	84.99	64.9
	3#15G1	12.22	101.3	51.6	13345	2341	51	C.C	68	20.64	109.83	55.8
	4#15G1	15.61	138.2	65.1	13489	1816	41	C.C	77	20.64	123.29	49.2
	2#15G2	11.22	95.93	62.9	14136	1454	32	C.C	73	17.81	94.74	50.8
	2#15G3	10.92	91.31	70	10277	2129	59	C.C	65	19.23	95.62	57.7
	6#15G1	11.98	118.3	42.6	7693	1976	65	C.C	92	19.14	120.21	39.8
	5#15G2	12.2	129.3	46.9	7550	2959	93	C.C	106	17.81	125.57	34.1
	5#15G3	12.61	110.6	40.7	6430	1839	74	C.C	95	19.22	128.70	38.9

: muhammad.rashid@univsul.edu.iq; faris.rashied@koyauniversity.org; serwan.rafiq@univsul.edu.iq
[1]Corresponding author: College of Engineering, University of Sulaimani, Kurdistan Region, Iraq.

	2#20G1	15.36	107.4	68.2	13372	2090	46	C.C	69	20.64	110.47	54.9
	3#20G1	16.32	140.4	61.5	6794	3087	106	C.C	81	21.46	134.02	47.2
	2#22G1	12.88	132.3	53.5	13651	2646	55	C.C	74	20.64	117.50	51.2
	3#20G2	12.29	171.4	59	11823	2648	62	C.C	81	22.94	146.55	47.0
	2#25G1	11.32	161.7	60	10028	2529	68	C.C	83	22.94	147.91	46.1
	2#25G2	16.77	167.2	53.3	7573	2045	72	C.C	91	22.94	160.93	41.8
	2#25G3	13.2	115.9	40.7	6429	1627	68	C.C	96	19.22	133.30	38.6
Wang & Belarbi	P4G-1	NG	46	26.2	11470	3000	38	C.C	47	6.68	40.36	18.8
(2011)	P8G-1	NG	50.9	24.4	8250	2800	45	C.C	54	6.68	44.19	16.0
Toutanji & Deng	GB1-1	11.7	60	70	NG	NG	NG	C.C	40	9.90	43.39	47.0
(2003)	GB1-2	12.3	59	73	NG	NG	NG	C.C	40	9.90	43.39	47.0
	GB2-1	13.4	65	60	NG	NG	NG	C.C	48	9.90	51.51	39.4
	GB2-2	12.8	64.3	59	NG	NG	NG	C.C	48	9.90	51.51	39.4
	GB3-1	11.8	71	61	NG	NG	NG	C.C	53	9.90	53.52	35.2
	GB3-2	11.6	70.5	62	NG	NG	NG	C.C	53	9.90	53.52	35.2
El Refai et al	2G12	NG	49.03	105.2	NG	NG	NG	G.R	34	13.53	47.58	105.4
(2015)	3G12	NG	53.78	108.2	NG	NG	NG	C.C	42	13.53	56.62	89.9
	3G16	NG	69.55	81	NG	NG	NG	C.C	53	13.53	70.76	70.7
Barris et al	C-212-D1	NG	38.22	52.2	NG	NG	NG	C.C	35	4.04	24.24	28.0
(2009)	C-216-D1	NG	45.06	40.5	NG	NG	NG	C.C	46	3.92	29.17	21.2
	C-316-D1	NG	49.38	32.5	NG	NG	NG	C.C	54	3.88	33.43	18.0
	C-212-D2	NG	27.69	47.8	NG	NG	NG	C.C	34	3.76	18.11	27.2
	C-216-D2	NG	42.15	45.4	NG	NG	NG	C.C	38	4.69	26.79	25.1
	C-316-D2	NG	43.2	38.6	NG	NG	NG	C.C	46	4.63	30.60	21.1
Goldston et al	40#2-0.5-S	1.00	4.6	52.2	G.F	1400	NG	B.F	17	1.47	5.48	62.3
(2016)	40#3-1.0-S	1.67	13.1	60.4	12000	2900	25	C.C	30	1.47	8.87	37.6
	40#4-2.0-S	1.93	16.6	59.9	9800	3300	31	C.C	36	1.47	10.28	31.1
	80#2-0.5-S	1.20	5.17	54.5	G.F	1000	NG	G.R	10	2.08	5.77	58.5
	80#3-1.0-S	1.97	14.2	56.3	G.F	2200	NG	C.C	24	2.08	12.32	49.9
	80#4-2.0-S	1.90	16.5	47.3	9300	2700	28	C.C	28	2.08	14.48	41.5
Adam et al	A25-1	5.61	25.25	84	13000	NG	NC	G.R	34	4.94	13.58	38.6
(2015)	A25-2	5.94	22.39	55	14000	NG	NC	SG.R	42	4.94	16.69	32.6
	A25-3	5.99	41.36	90	17000	NG	NC	C.C	54	4.94	20.72	26.3
	A45-1	8.69	30.69	80	15000	NG	NC	G.R	32	6.92	23.38	44.5
	A45-2	8.47	45.05	85	15000	NG	NC	C.C	41	6.92	29.41	36.2
	A45-3	9.68	60.39	78	15000	NG	NC	C.C	52	6.92	36.04	29.4
	A70-1	8.97	46.53	88	13000	NG	NC	G.R	37	8.61	34.49	41.1
	A70-2	8.53	72.99	95	13000	NG	NC	C.C	46	8.61	42.57	33.7
	A70-3	10.95	79.81	92	13000	NG	NC	C.C	54	8.61	48.42	28.6

Note, C.C is top fiber concrete crushing, G.R is GFRP rupture, B.F is balanced failure of both top and GFRP at the same time, G.F. is strain gauge failure, NG is not available in the reference, NC cannot be calculated due to

: muhammad.rashid@univsul.edu.iq; faris.rashied@koyauniversity.org;
serwan.rafiq@univsul.edu.iq

[1]Corresponding author: College of Engineering, University of Sulaimani, Kurdistan Region, Iraq.

lack of concrete strain, SG.R is suddenly GFRP failure before reaching its tested tensile strength.

Figure 2 shows the ratio of experimental to ACI 440 predicted nominal moment capacities $M_{n,exp}/M_n$ at failure. the majority of ratios evidently presented that ACI 440.1R-15 underestimated the calculated flexural moment compared to the experimental load carrying capacity. The moment ratios varied between o.84 and 2 with the mean value of 1.25. Among 53 beams, 77% of their moment ratios were greater than 1 while the remaining moment ratios (23%) ranged between 0.84 and 1. All the moment ratios obtained from (Toutanji and Deng 2003, Barris et al 2009, Kassem et al 2011, Wing & Belari 2011, Adem et al 2015) showed that GFRP reinforced concrete beams can carry loads more than those predicted by ACI 440. ρ_f mostly differs from 0.34% to 2.32%. Looking at the moment ratios calculated from (Goldston et al 2016), the ratios increased with increasing GFRP reinforcement ratio. For instance, it was 0.84 at ρ_f = 0.5% and considerably reached 1.62 at ρ_f = 2%. However, there is no clear trend between ρ_f and $M_{n,exp}/M_n$ considering different works due to fluctuation of the moment ratios along ρ_f. Because the failure of the beams was concrete crushing the increased reinforcement ratio did not have significant effect on moment capacity of the beams.

Regarding midspan ultimate deflections at failure, Figure 3 shows the deflection ratios $\Delta_{n,exp}/\Delta_n$ between the experimental deflection to theoretical deflection obtained from ACI 440. It was observed that ultimate deflections calculated by ACI 440 underestimated the deflection compared to the experimental observations. The deflection ratios ranges between 0.84 and 3.32 with an average of 1.55. It can be noted that 7 out of 9 moment ratios obtained from (Adam et al 2015) reached above 2, whereas all remaining moment ratios obtained were under 2. A major number of tested beams (94%) revealed that the theoretical deflections undervalued less than those measured in the laboratory. Figure 3 also gives the ratios of effective to gross moment of inertia I_e/I_g corresponding to their ultimate moment ratios, frequently ranged between 0.04 and 0.22. due to the geometrical variety of specimens, the dispersions of $\Delta_{n,exp}/\Delta_n$ occurs and it is weak to establish equation between both ratios.

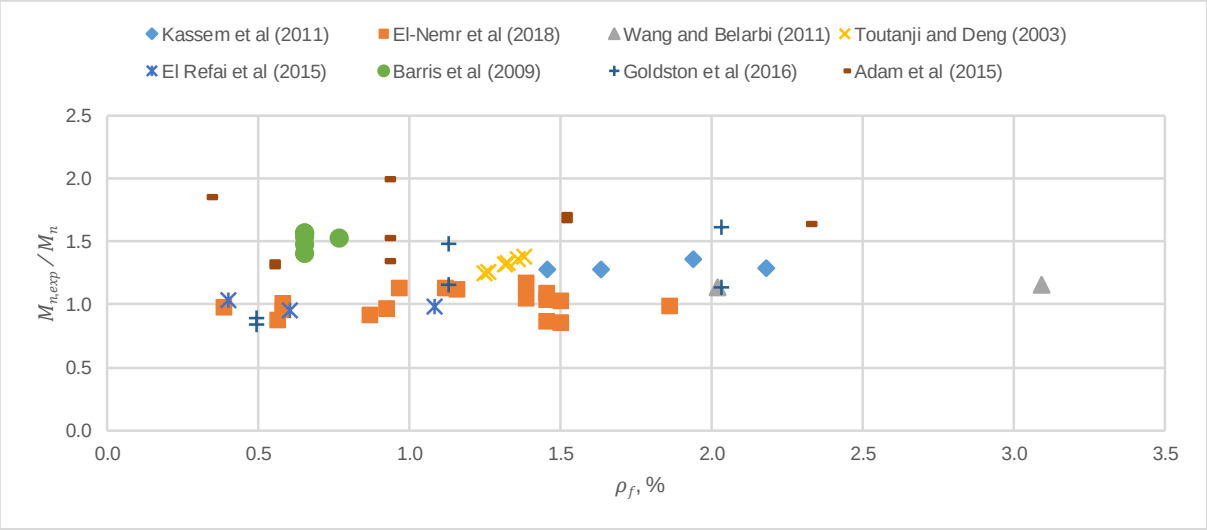

Fig. (2): Experimental to predicted nominal moment ratio versus GFRP reinforcement ratio

: muhammad.rashid@univsul.edu.iq; faris.rashied@koyauniversity.org; serwan.rafiq@univsul.edu.iq

[1]Corresponding author: College of Engineering, University of Sulaimani, Kurdistan Region, Iraq.

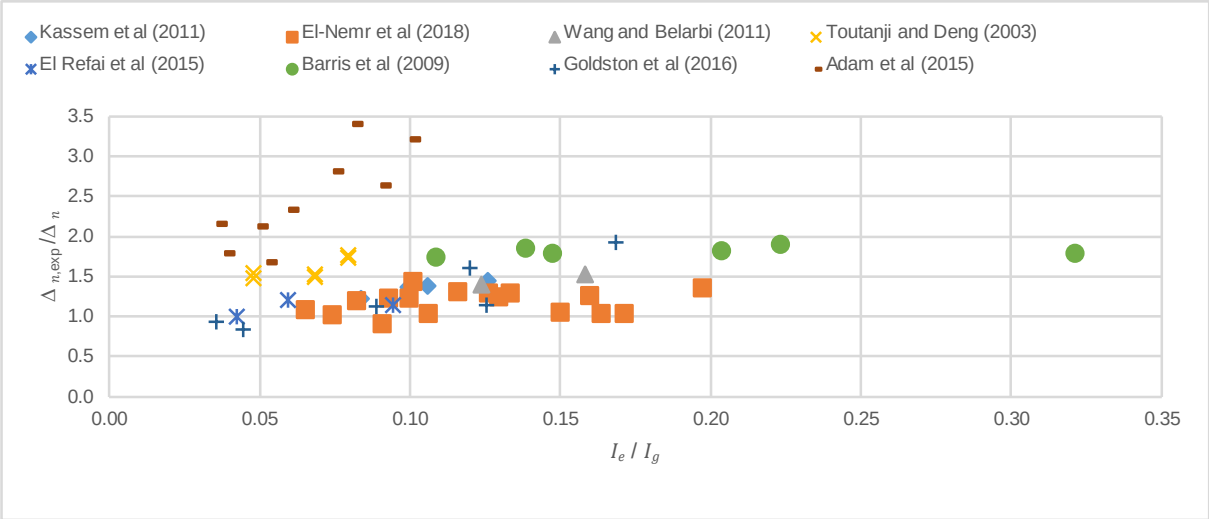

Fig. (3): Experimental to predicted ultimate deflection ratio versus gross to effective sectional moment ratio

Figure 4 shows the ratios of experimental cracking moment at $P_{cr,exp}$ to theoretical cracking moment calculated by Equation (17) at P_{cr} with respected to theoretical flexural strength of concrete estimated by Equation (15). The concrete flexural strength is the controlling parameter for calculating cracking moment. All experimental cracking moments obtained by (Kassem et al 2011, EL-Nemr et al (2018) were less than those predicted by ACI 440, whereas they were conservative according to Toutanji and Deng (2003). The cracking moment data were available for 42 beams. It can be seen that $M_{cr,exp}/M_{cr}$ ratios vary between 0.49 and 1.4 with an average of 0.92. Regarding to the cracking deflection ratio $\Delta_{cr,exp}/\Delta_{cr}$, Only two of the works stated cracking deflections for their tested beams. El-Nemr et al (2018) reported that first crack occurs at the deflections of less than 3 mm without reporting the data. Kassem et al (2011) presents that the cracking deflections for the beams G1-6, G1-8, G2-6, and G2-8 were (2.9, 2.8, 3.2 and 3) mm, respectively while theoretical cracking deflection calculated from Equation (29) is equal to 0.72 mm. The experimental cracking deflection are about four times greater than those calculated by ACI 440. There are two main reasons for the difference between both theoretical and experimental results. Firstly, the flexural tensile of concrete $f_r = 0.62\lambda\sqrt{f_c'}$ could be various from the actual flexural strength of the concrete. Secondly, the experimental cracking deflection cannot have observed at pre-cracking loads and the beam already cracked. In this critical situation, I_g that is used in the calculation of theoretical deflection is more than that moment of inertia of the beam.

: muhammad.rashid@univsul.edu.iq; faris.rashied@koyauniversity.org;
serwan.rafiq@univsul.edu.iq
[1]Corresponding author: College of Engineering, University of Sulaimani, Kurdistan Region, Iraq.

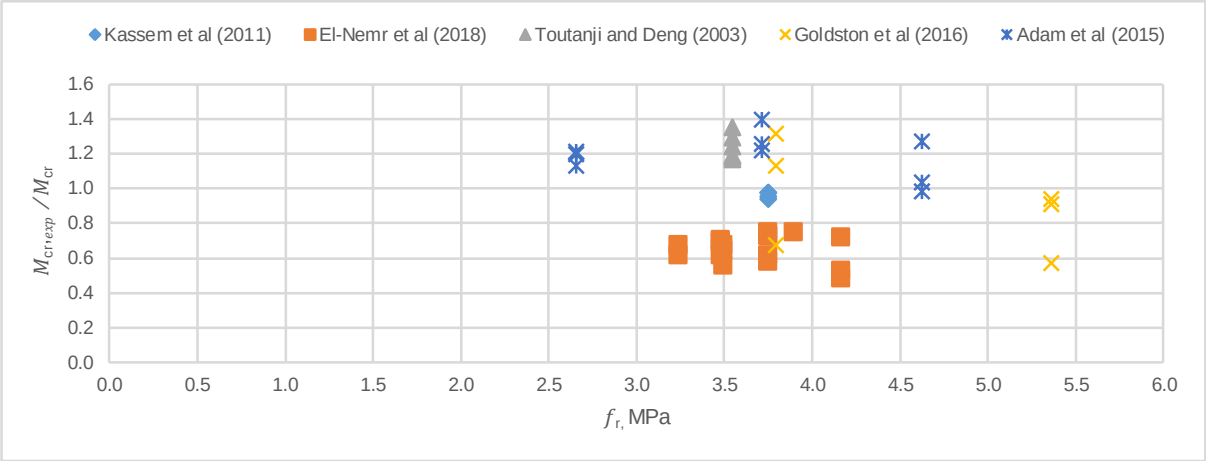

Fig. (4): Experimental to predicted cracking moment ratio versus concrete flexural strength

Figure 5 presents the ratios of the experimental neutral axis depth to theoretical neural axis depth of the beam section at failure. The experimental neutral axis depths were calculated by Equation (30) on the basis of strains measured by the top and bottom strain gauges. Due to lack of data and strain gauge ruptures, among 53 beams, experimental neutral axis can be found for 26 beams. The results showed that experimental neural axis depth were less than the theoretical values except 3#20G1. Without considering outliers, the experimental to predicted neutral axis depth ratios ranges between 0.527 to 0.989 with an average with 0.786. The reason for these decreased neural depth ratios belongs to concrete crushing failure, and adopted equivalent rectangular stress block parameters (α and β_1) from ACI 318. It can be noted that β_1 is limited to 0.65 beyond cylindrical compressive strength of 55 MPa. The results revealed that equivalent rectangular stress block parameters need to be adjusted for GFRP reinforced concrete member.

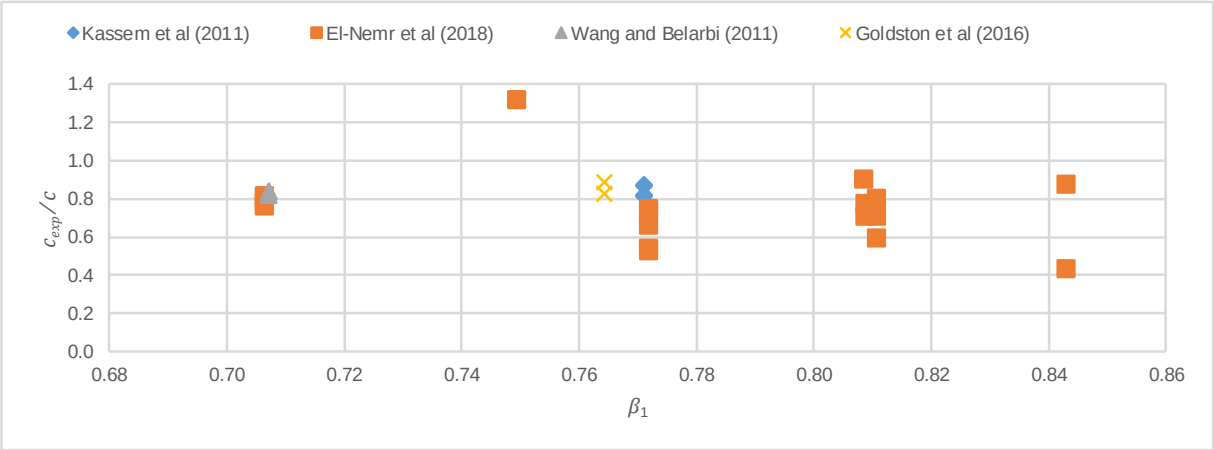

Fig. (5): Experimental to predicted neutral axis depth ratio versus an equivalent stress block parameter

The statistical data analysis provided by box and whisker method showed to the represented values such mean, median, first and second quadrantes, outliers for the ratios of the experimental to theoretical ultimate moment, cracking moment, ultimate deflection and

: muhammad.rashid@univsul.edu.iq; faris.rashied@koyauniversity.org; serwan.rafiq@univsul.edu.iq
[1]Corresponding author: College of Engineering, University of Sulaimani, Kurdistan Region, Iraq.

neutral axis depth as shown in Figure 6. Except the cracking moment ratios, the other ratios had outliers, which taken out of the calculated median. For instance, the outliers for ultimate deflection ratios were 2.82, 3.22 and 3.42. According to the analysis and based on the median of the values, the modification factors are estimated to be used during design. The modification factor for the experimental to ACI 440.1R-15 ultimate moment, cracking moment, ultimate deflection and neutral axis depth can be 1.25, 0.94, 1.4 and 0.806, respectively in addition, these areas required standardizing the manufacturing process of GFRP bar internationally to avoid the market discrepancies.

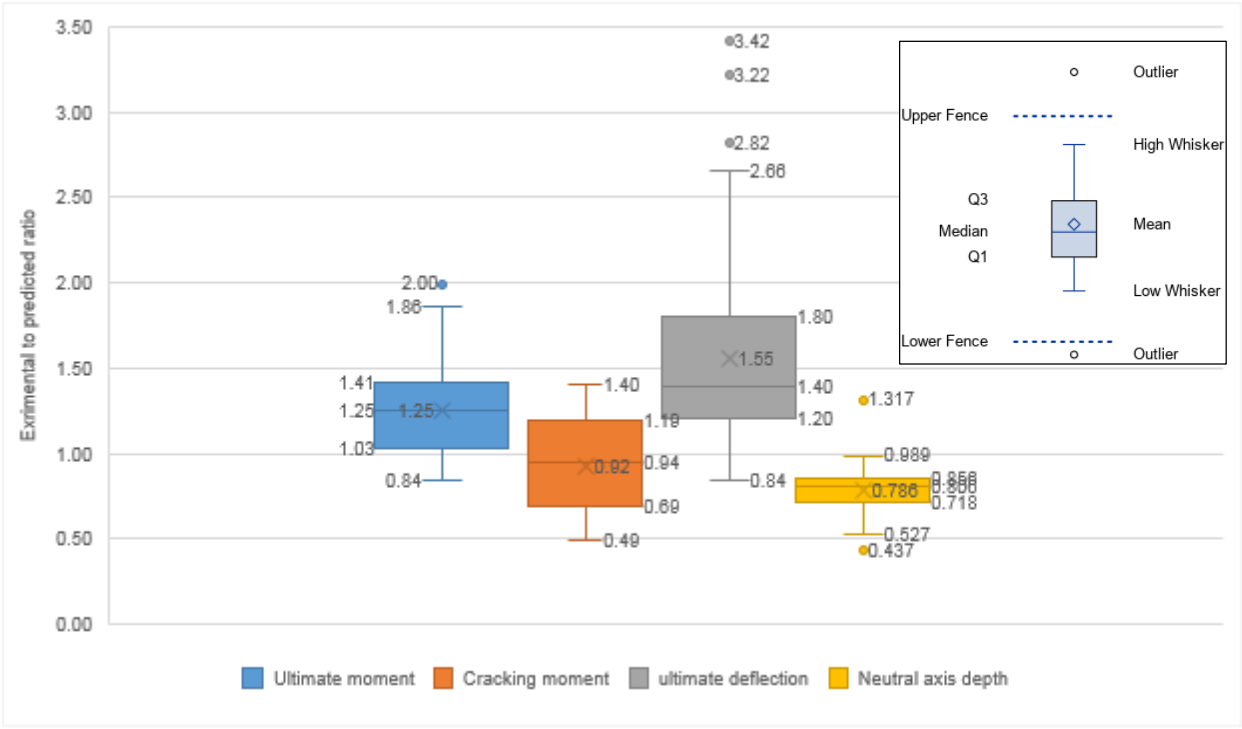

Fig. (6): Statistical data analysis according to box and whisker method

5. CONCLUSION

Investigational test results of 53 GFRP reinforced concrete beams that tested under four-point loading test to failure were gathered from the literature. The concrete beams covering a variety of dimensional properties were made of GFRP rebar for longitudinal flexural reinforcement and steel rebar for traverse reinforcement. The beam data selected from different studies, and GFRP rebars that used have different modulus of elasticity, tensile-strength, and GFRP reinforcement ratio and configuration. The investigational results were compared with those predicted by ACI 440.1R-15 in terms of the cracking and flexural moments, cracking and ultimate deflections, and neural axis depth. On the basis of the experimental and theoretical results, the following conclusions can be drawn:

- The database of 53 GFRP reinforced concrete beam with dimensional and materials properties have been collected, which tested by others with pure bending flexural test and failed in flexure.
- Due to lack of a comprehensive numerical detail in the literature, an understanding approach has been presented to compute the experimental deflection and flexural capacity compared with the theoretical equations given in ACI 440.1R-15, which has provided new researchers with an adequate starting in the field.

: muhammad.rashid@univsul.edu.iq; faris.rashied@koyauniversity.org;
serwan.rafiq@univsul.edu.iq
[1]Corresponding author: College of Engineering, University of Sulaimani, Kurdistan Region, Iraq.

• Nominal moment capacity has been negligibly affected by increasing GFRP reinforcement ratios because GFRP reinforcement ratios were greater than GFRP balanced ratio while the concrete crushed controlled failure mode. The investigational results showed underestimate of ultimate moment achieved by ACI 440. The modification factor (1.25) has been predictable.

• Three beams have failed in GFRP rupture while their GFRP reinforcement ratios were greater than the balanced reinforcement ratios up to $1.46\rho_{fb}$. To ensure compression failure , it has been given to use more than $1.5\rho_{fb}$.

• GFRP reinforced concrete beams experienced the experimental ultimate deflections more than those calculated by ACI 440. The variances have reached up to 3.5 times, and the modification factor was proposed to be 1.4.

• The majority of the experimental cracking moments was commonly less than the predicted results. However, the cracking moment ratios are close and the justification value of 0.94 was proposed. In addition, for the available data it has been concluded that the predicted cracking deflections were underestimated.

• The experimental results have given the neural axis depth less than those obtained from theoretical calculation. The value of 0.806 has been assessed to justify the predicted neutral axis depth. it has been concluded that the main reason behind these gaps related to the equivalent rectangular stress block parameters

REFERENCES

ACI Committee 318 (2019). Building code requirements for structural concrete and commentary (ACI 318-19). Farmington Hills, MI: American Concrete Institute.

ACI Committee 440. (2015). Guide for the Design and Construction of structural concrete reinforced with Fiber Reinforced Polymer (FRP) bars (ACI 440.1 R-15). Farmington Hills, MI: American Concrete Institute.

Adam, M. A., Said, M., Mahmoud, A. A., & Shanour, A. S. (2015). Analytical and experimental flexural behavior of concrete beams reinforced with glass fiber reinforced polymers bars. Construction and Building Materials, 84, 354-366.

Alsayed, S. H., Al-Salloum, Y. A., & Almusallam, T. H. (2000). Performance of glass fiber reinforced plastic bars as a reinforcing material for concrete structures. Composites Part B: Engineering, 31(6-7), 555-567.

Ashour, A. F. (2006). Flexural and shear capacities of concrete beams reinforced with GFRP bars. Construction and Building Materials, 20(10), 1005-1015.

Bank, L. C. (2006). Composites for construction: structural design with FRP materials. John Wiley & Sons.

Barris, C., Torres, L., Turon, A., Baena, M., & Catalan, A. (2009). An experimental study of the flexural behaviour of GFRP RC beams and comparison with prediction models. Composite Structures, 91(3), 286-295.

Benmokrane, B., Chaallal, O., & Masmoudi, R. (1995). Glass fibre reinforced plastic (GFRP) rebars for concrete structures. Construction and Building Materials, 9(6), 353-364.

Bischoff, P. H. (2005). Reevaluation of deflection prediction for concrete beams reinforced with steel and fiber reinforced polymer bars. Journal of structural engineering, 131(5), 752-767.

Burgoyne, C. J., Byars, E., Guadagnini, M., Manfredi, G., Neocleous, K., Pilakoutas, K., ... & Al Sunna, R. (2007). FRP reinforcement in RC structures.

El Refai, A., Abed, F., & Al-Rahmani, A. (2015). Structural performance and serviceability of concrete beams reinforced with hybrid (GFRP and steel) bars. Construction and Building Materials, 96, 518-529.

El-Nemr, A., Ahmed, E. A., El-Safty, A., & Benmokrane, B. (2018). Evaluation of the

: muhammad.rashid@univsul.edu.iq; faris.rashied@koyauniversity.org; serwan.rafiq@univsul.edu.iq

[1]Corresponding author: College of Engineering, University of Sulaimani, Kurdistan Region, Iraq.

flexural strength and serviceability of concrete beams reinforced with different types of GFRP bars. Engineering Structures, 173, 606-619.

Emparanza, A. R., Kampmann, R., De Caso, Y., & Basalo, F. (2018). State-of-the-Practice of Global Manufacturing of FRP Rebar and Specifications. Special Publication, 327, 45-1.

Goldston, M., Remennikov, A., & Sheikh, M. N. (2016). Experimental investigation of the behaviour of concrete beams reinforced with GFRP bars under static and impact loading. Engineering Structures, 113, 220-232.

Kalpana, V. G., & Subramanian, K. (2011). Behavior of concrete beams reinforced with GFRP BARS. Journal of reinforced plastics and composites, 30(23), 1915-1922.

Kassem, C., Farghaly, A. S., & Benmokrane, B. (2011). Evaluation of flexural behavior and serviceability performance of concrete beams reinforced with FRP bars. Journal of Composites for Construction, 15(5), 682-695.

Tighiouart, B., Benmokrane, B., & Gao, D. (1998). Investigation of bond in concrete member with fibre reinforced polymer (FRP) bars. Construction and building materials, 12(8), 453-462.

Toutanji, H. A., & Saafi, M. (2000). Flexural behavior of concrete beams reinforced with glass fiber-reinforced polymer (GFRP) bars. Structural Journal, 97(5), 712-719.

Toutanji, H., & Deng, Y. (2003). Deflection and crack-width prediction of concrete beams reinforced with glass FRP rods. Construction and Building Materials, 17(1), 69-74.

Wang, H., & Belarbi, A. (2011). Ductility characteristics of fiber-reinforced-concrete beams reinforced with FRP rebars. Construction and Building Materials, 25(5), 2391-2401.

: muhammad.rashid@univsul.edu.iq; faris.rashied@koyauniversity.org;
serwan.rafiq@univsul.edu.iq
[1]Corresponding author: College of Engineering, University of Sulaimani, Kurdistan Region, Iraq.